# Ultrafine Pt Nanoparticle Decorated NiRu-BDC Nanosheets as Bifunctional Electrocatalysts for Alkaline Hydrogen Evolution and Methanol Oxidation

Binghao Chen, Yilun Gao, Dongyang Zhang, Jiahui Xiang and Binbin Fan*

Shandong Key Laboratory of Renewable Membrane Materials, Collage of Materials Science and Engineering, Qingdao University, Qingdao 266071, China

E-mail: fanbb1991@qdu.edu.cn

## Experimental Section

### Preparation of Pt@NiRu-BDC/NF, Pt@Ni-BDC/NF, and Ni-BDC/NF.

In a typical synthesis, 1 mmol of $Ni(NO_3)_2 \cdot 6H_2O$ and 0.5 mmol of $H_2PtCl_6 \cdot 6H_2O$ were dissolved in 7.5 mL of DMF. $RuCl_3$ (0.5, 1.0, 1.5, or 2.0 mmol) was then added to the above solution. The mixture was transferred to a 25 mL stainless-steel reactor and heated at 100 °C for 7 h. After cooled to room temperature, the products were obtained and denoted as Pt@$NiRu_{0.5}$-BDC/NF, Pt@$NiRu_1$-BDC/NF, Pt@$NiRu_{1.5}$-BDC/NF, and Pt@$NiRu_2$-BDC/NF, respectively. Pt@Ni-BDC/NF was prepared by the same procedure but without $RuCl_3$. Ni-BDC/NF was prepared without both $H_2PtCl_6 \cdot 6H_2O$ and $RuCl_3$.

### Materials Characterization

To investigate the morphology and structure of the catalysts, scanning electron microscopy (SEM), transmission electron microscopy (TEM), atomic force microscopy (AFM), and powder X-ray diffraction (XRD) were employed. SEM was performed on a JEOL JSM-7800F microscope, TEM on a JEOL 2100Plus, AFM on a Bruker Dimension Icon, and XRD on a Bruker D8 Advance. TEM samples were prepared by drop-casting ethanol dispersions of the nanocrystals onto carbon-coated copper grids. Crystal structures were analyzed by powder XRD. X-ray photoelectron spectroscopy (XPS) was carried out on a Thermo Fisher Scientific ESCALAB 250 instrument using a monochromatic Al Kα source.

### Preparation Pt/C electrodes

For the Pt/C electrode, 10 mg of Pt/C was dispersed in 950 μL of isopropanol and 50 μL of Nafion solution to form a homogeneous slurry, which was then drop-cast onto nickel foam to achieve a mass loading of 2 mg $cm^{-2}$.

### Electrochemical measurement.

Electrochemical measurements were performed using a CHI 760E electrochemical workstation in a standard three-electrode configuration, comprising a working electrode, an Ag/AgCl (saturated KCl) reference electrode, and a platinum sheet counter electrode. For HER and MOR evaluations, the as prepared Pt@NiRu-BDC/NF, Pt@Ni-BDC/NF, and Ni-BDC/NF MOF-based electrocatalysts were directly employed

as the working electrodes. The total catalyst mass loading was uniformly maintained at 2 mg across all samples, with the Pt content determined according to the following equation:

$$m_{Pt} = Catalyst\ Mass \times Pt_{Mass\ Percentage} \quad (1)$$

The mass activity was calculated by normalizing the peak current obtained from the MOR polarization curves to the total mass of Pt loaded on the working electrode:

$$J_{Mass} = \frac{I}{m_{Pt}} \quad (2)$$

The specific Pt loadings for different samples are detailed in Table S1.

All potentials reported in this study were referenced to the reversible hydrogen electrode (RHE) using the equation: $E_{RHE}=E_{Ag/AgCl} + 0.059pH + 0.198$.

For the methanol oxidation reaction (MOR) in alkaline media, the overall reaction follows a six-electron transfer process:

$$CH_3OH + 6OH^- \rightarrow CO_2 + 5H_2O + 6e^- \quad (3)$$

The theoretical Faradaic efficiency is defined as:

$$FE = \frac{n\ F\ n_{product}}{Q_{product}} \times 100\% \quad (4)$$

Where n is the number of electrons transferred, F is the faradic constant (96485 C/mol), is the molar amount of the product.

The ECSA was estimated based on the electric double-layer capacitance (Cdl) method. Cyclic voltammetry (CV) was performed in a non-Faradaic potential region (0.45~0.7V) at various scan rates ( 20, 40, 60, 80, 100, and 120 mV $s^{-1}$). The Cdl was determined plotting the capacitive current density against the scan rate, where the slope represents.

**Methanol Oxidation Reaction (MOR) Measurements:** MOR characterization was carried out in an electrolyte containing 1.0 M KOH and 1.0 M $CH_3OH$. CV profiles were recorded at 50 mV $s^{-1}$, and LSV curves were acquired at 5 mV $s^{-1}$ within the potential range of 0.4 to 1.2 V. Catalytic stability was evaluated by 1,000 CV cycles in the same electrolyte. CO stripping experiments were performed in 1.0 M KOH. Prior to measurement, the electrolyte was deaerated by purging with high-purity $N_2$ for 10

min, followed by electrochemical activation via 20 CV cycles at 50 mV $s^{-1}$. CO was then adsorbed onto the electrode surface by bubbling CO gas into the cell at a constant potential of 0.1 V for 10 min. After CO saturation, the electrolyte was purged with $N_2$ for an additional 10 min to remove dissolved CO. Finally, CV was conducted from 0 to 1.36 V vs. RHE to obtain the CO stripping voltammograms.

**Hydrogen Evolution Reaction (HER) Measurements:** HER tests were conducted in 1.0 M KOH electrolyte. CV curves were performed at a scan rate of 50 mV $s^{-1}$, and LSV curves were recorded at 5 mV $s^{-1}$ within a potential window of -0.17 to 0.23 V vs. RHE. All polarization curves were corrected with 95% iR compensation. Electrochemical durability was measured by chronoamperometry at the overpotential of 48 mV.

**In situ Raman measurements**

In this study, the potential was controlled within the range of 0.78-1.18 V vs. RHE. Raman spectra were collected over a wavenumber range of 800-3000 $cm^{-1}$, with an integration time of 5 s, 5 accumulations at each potential, and a laser power set to 50%.

**Table S1.** Summary of elemental analysis obtained using EDS.

| Sample | C element Wt (%) | O element Wt (%) | Pt element Wt (%) | Ni element Wt (%) | Ru element Wt (%) |
|---|---|---|---|---|---|
| Pt@Ni-BDC/NF | 63.4 | 25.64 | 1.35 | 9.61 | 0 |
| Pt@$NiRu_{0.5}$-BDC/NF | 62.71 | 23.56 | 0.81 | 11.01 | 1.91 |
| Pt@$NiRu_1$-BDC/NF | 61.64 | 23.4 | 0.83 | 12.02 | 2.11 |
| Pt@$NiRu_{1.5}$-BDC/NF | 61.93 | 24.86 | 0.87 | 9.41 | 2.93 |
| Pt@$NiRu_2$-BDC/NF | 62.22 | 24.29 | 0.91 | 8.85 | 3.73 |

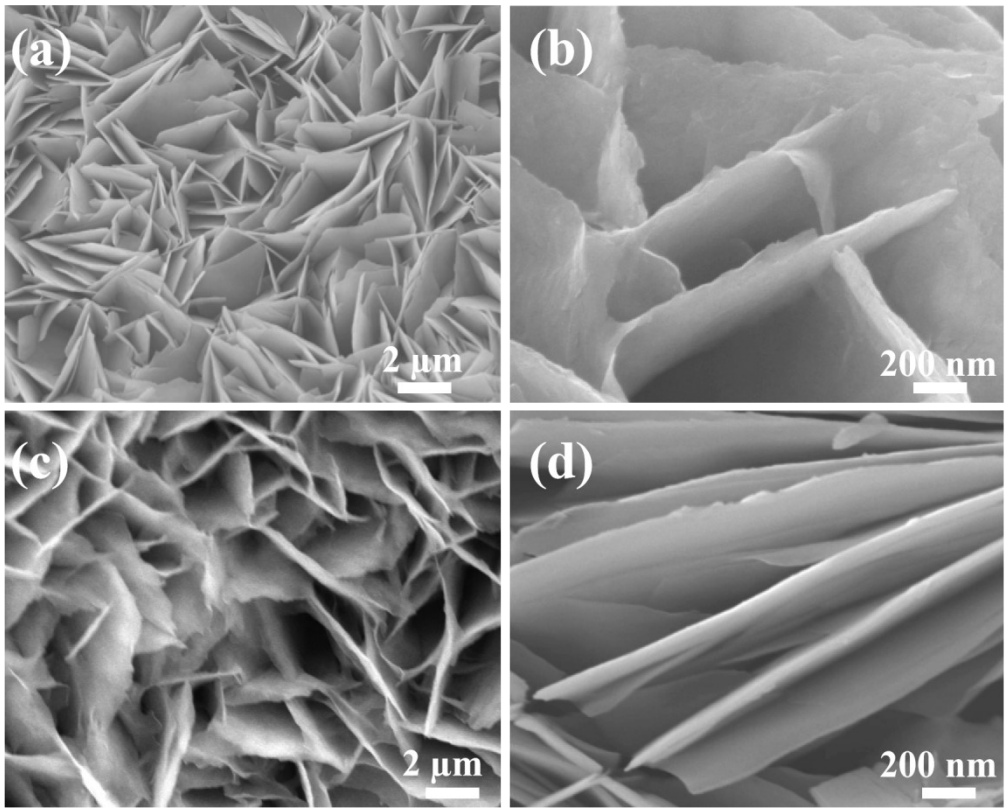


**Figure S1.** SEM images of (a, b) Ni-BDC/NF and (c, d) Pt@Ni-BDC/NF.

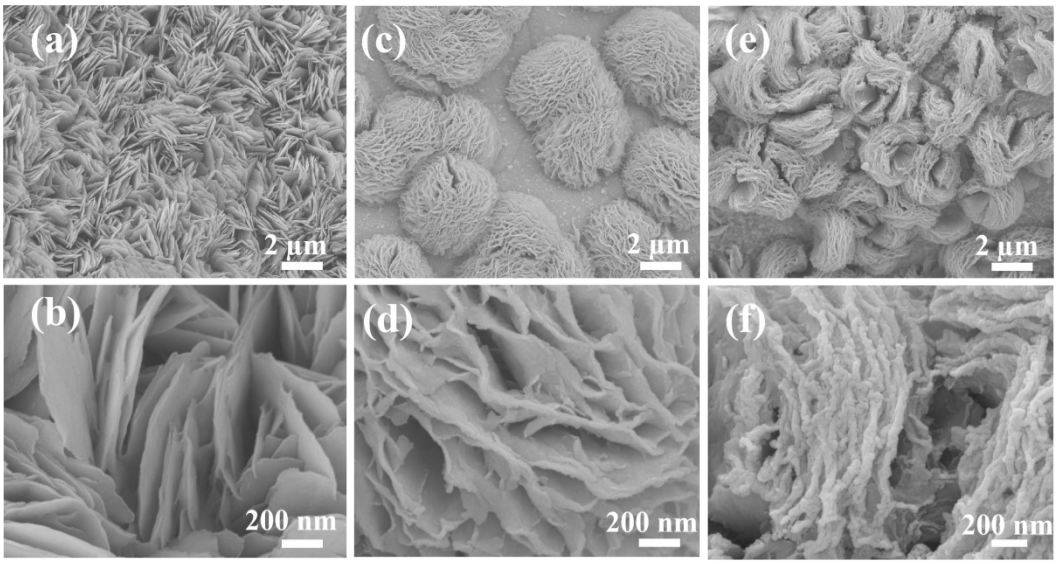


**Figure S2.** SEM images of (a, b) Pt@$NiRu_{0.5}$-BDC/NF, (c, d) Pt@$NiRu_{1.5}$-BDC/NF and (e, f) Pt@$NiRu_2$-BDC/NF.

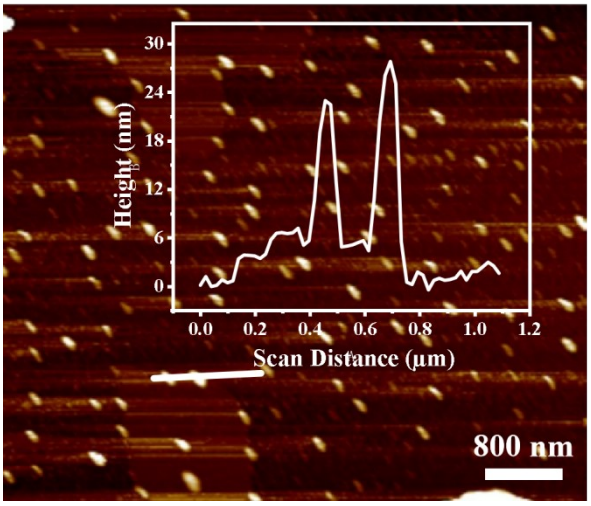


**Figure S3.** AFM image of Ni-BDC/NF (inset: thickness of nanosheets).

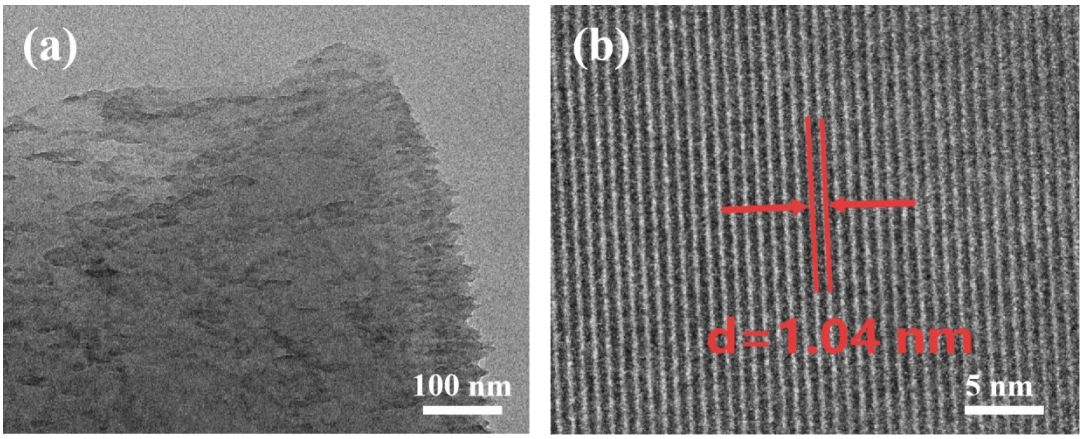


**Figure S4.** (a) TEM image of Ni-BDC/NF; (b) HRTEM image of Ni-BDC/NF.

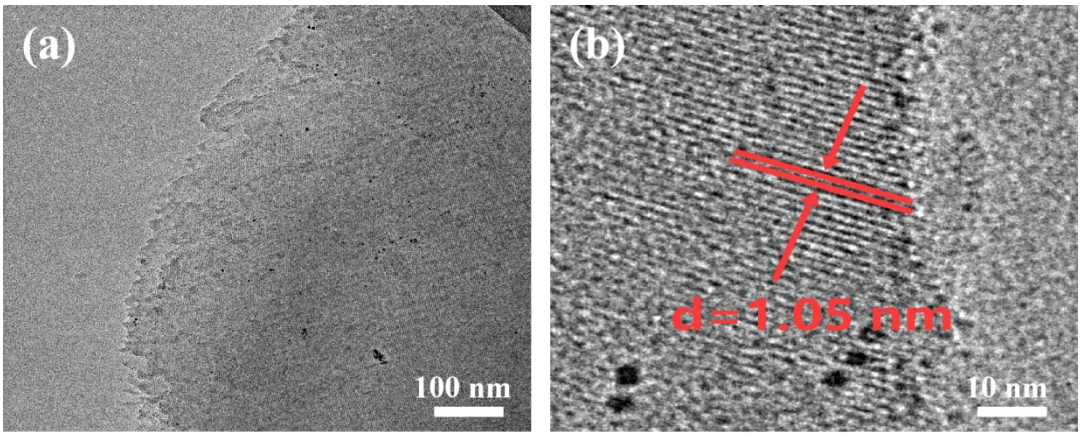


**Figure S5.** (a) TEM image of Pt@Ni-BDC/NF; (b) HRTEM image of Pt@Ni-BDC/NF.

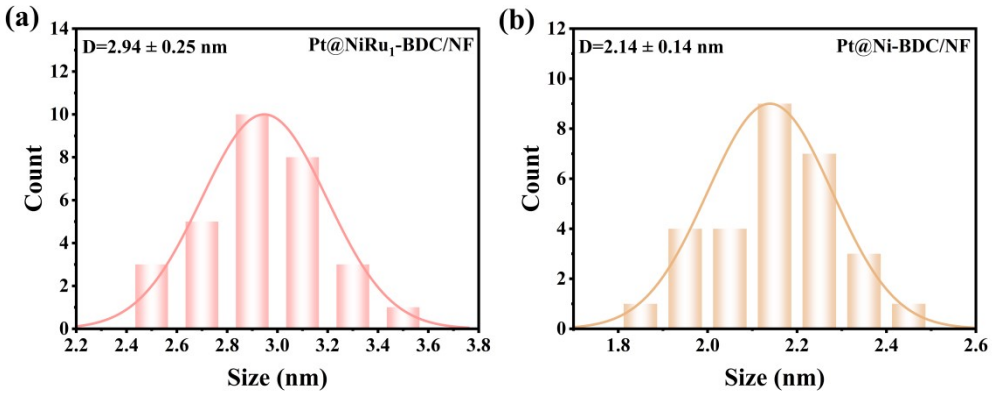


**Figure S6.** (a) Particle size distribution histogram of Pt nanoparticles in Pt@$NiRu_1$-BDC (Obtained from the nanoparticles in Fig. 1f); (b) Particle size distribution histogram of Pt nanoparticles in Pt@Ni-BDC (Obtained from the nanoparticles in Fig. S5a).

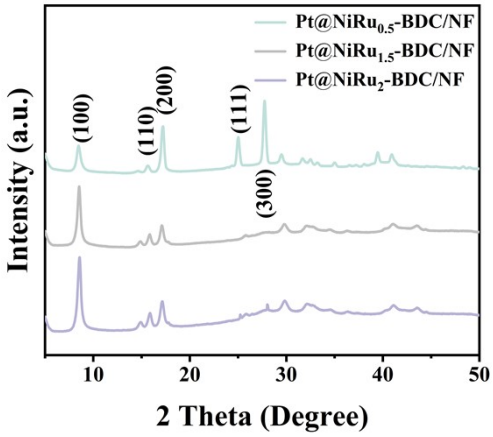


**Figure S7.** XRD patterns of Pt@$NiRu_{0.5}$-BDC/NF, Pt@$NiRu_{1.5}$-BDC/NF and Pt@$NiRu_2$-BDC/NF.

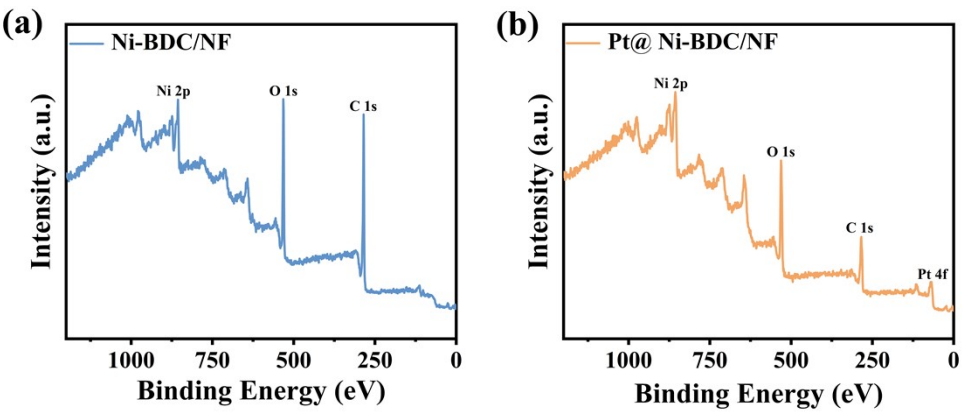


**Figure S8.** (a) The XPS survey spectra of Ni-BDC/NF; (b) The XPS survey spectra of Pt@Ni-BDC/NF.

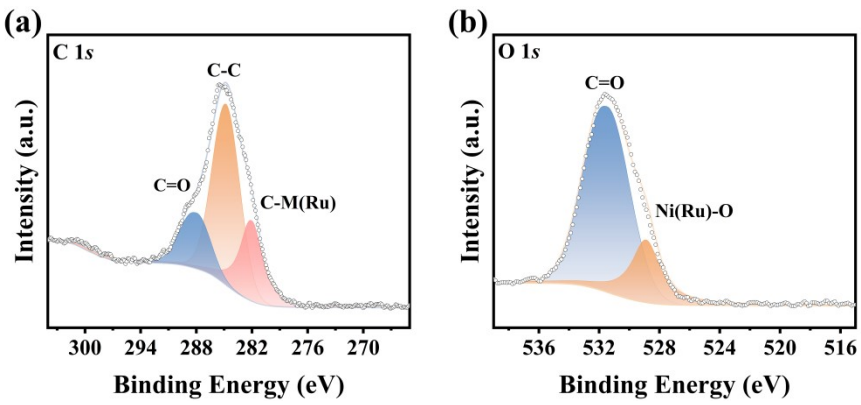


**Figure S9.** (a) High-resolution XPS spectra of C 1s for Pt@NiRu$_1$-BDC/NF; (b) High-resolution XPS spectra of O 1s for Pt@NiRu$_1$-BDC/NF.

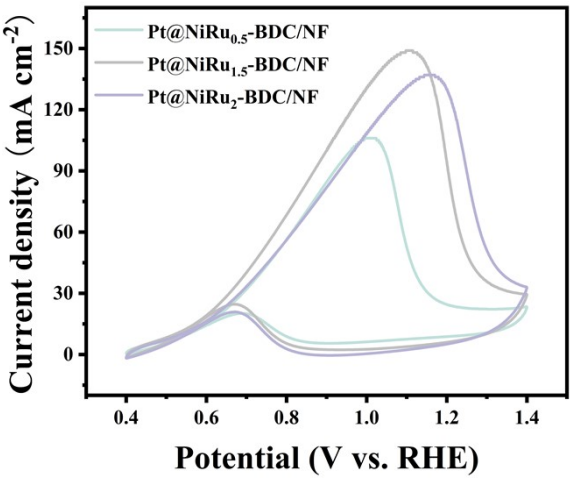


**Figure S10.** (a) CV curves of Pt@NiRu$_{0.5}$-BDC/NF, Pt@NiRu$_{1.5}$-BDC/NF and Pt@NiRu$_2$-BDC/NF in 1 M KOH + 1 M $CH_3OH$.

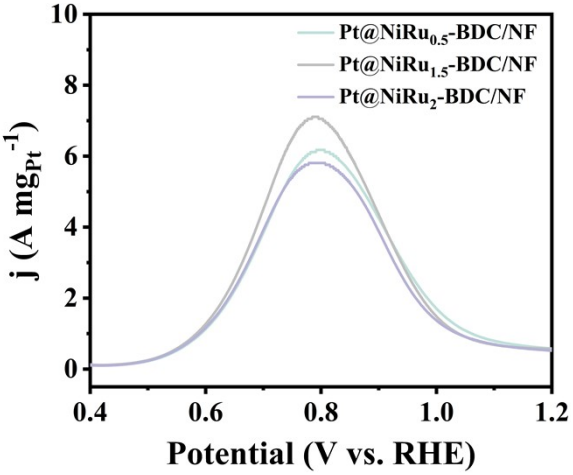


**Figure S11.** The mass activity of Pt@NiRu$_{0.5}$-BDC/NF, Pt@NiRu$_{1.5}$-BDC/NF and Pt@NiRu$_2$-BDC/NF electrocatalysts.

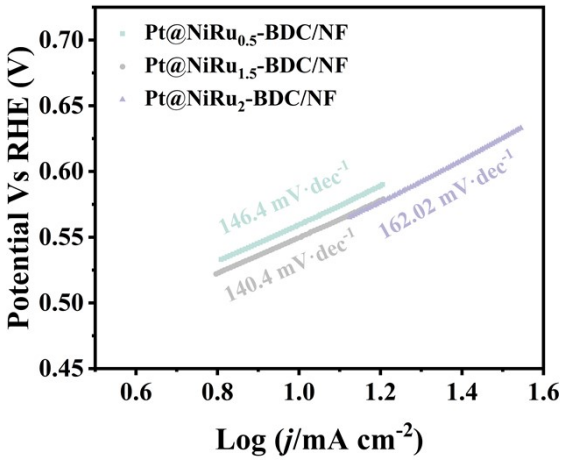


**Figure S12.** Tafel slopes of Pt@NiRu$_{0.5}$-BDC/NF, Pt@NiRu$_{1.5}$-BDC/NF and Pt@NiRu$_2$-BDC/NF electrocatalysts.

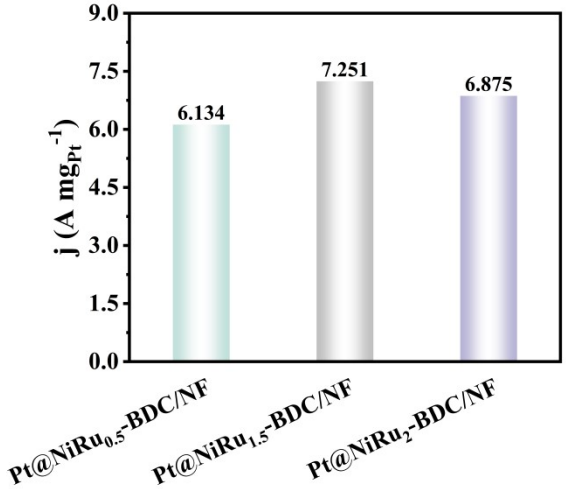


**Figure S13.** Mass activity for Pt@NiRu$_{0.5}$-BDC/NF, Pt@NiRu$_{1.5}$-BDC/NF and Pt@NiRu$_2$-BDC/NF electrocatalysts.

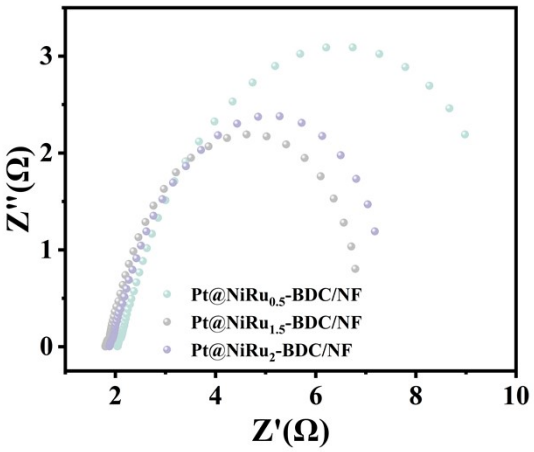


**Figure S14.** Impedance spectra of Pt@NiRu$_{0.5}$-BDC/NF, Pt@NiRu$_{1.5}$-BDC/NF and Pt@NiRu$_2$-BDC/NF electrocatalysts.

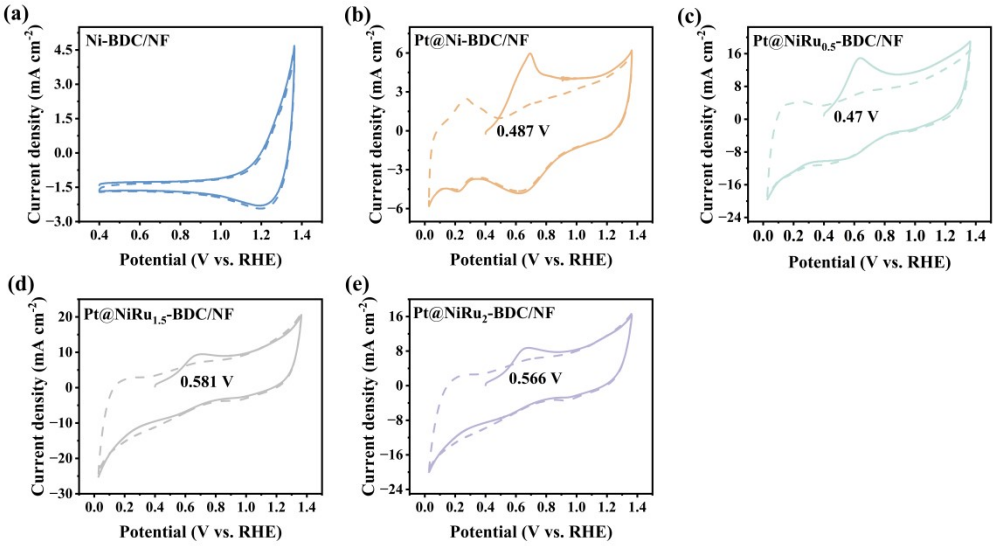


**Figure S15.** CO desorption curve of (a) Ni-BDC/NF, (b) Pt@Ni-BDC/NF, (c) Pt@NiRu$_{0.5}$-BDC/NF, (d) Pt@NiRu$_{1.5}$-BDC/NF and (e) Pt@NiRu$_2$-BDC/NF.

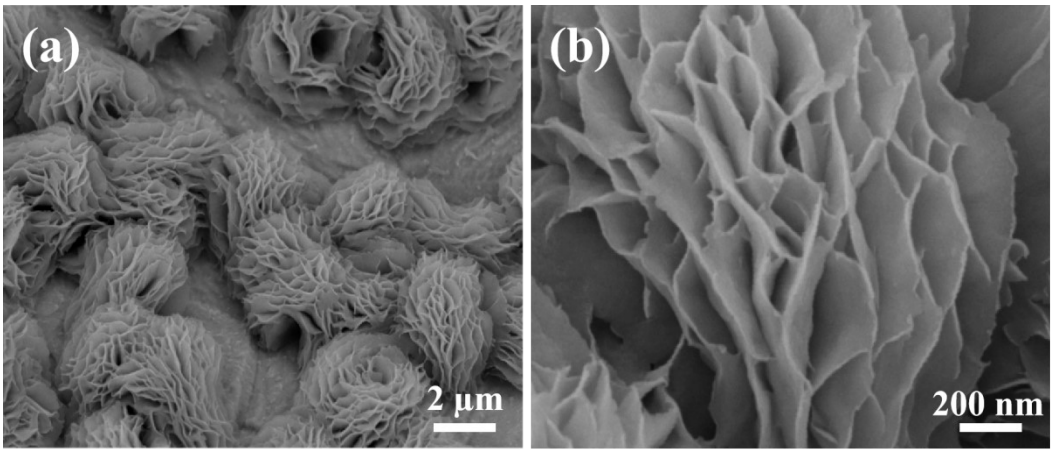


**Figure S16**. SEM images of Pt@NiRu$_1$-BDC/NF after MOR cycling stability measurements.

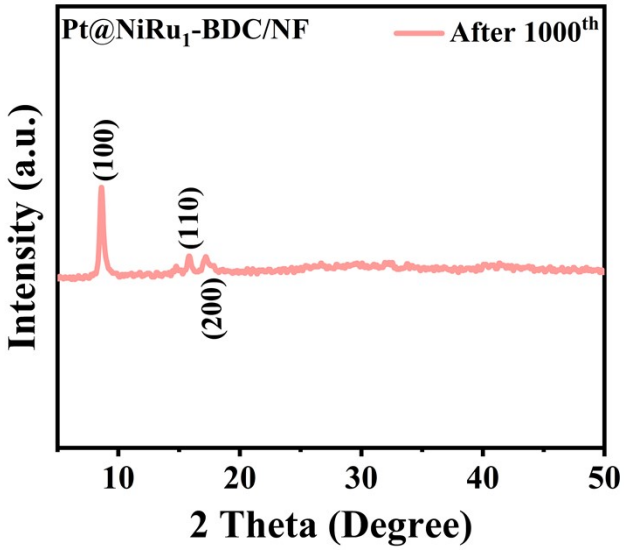


**Figure S17.** XRD patterns of Pt@NiRu$_1$-BDC/NF after MOR cycling stability test.

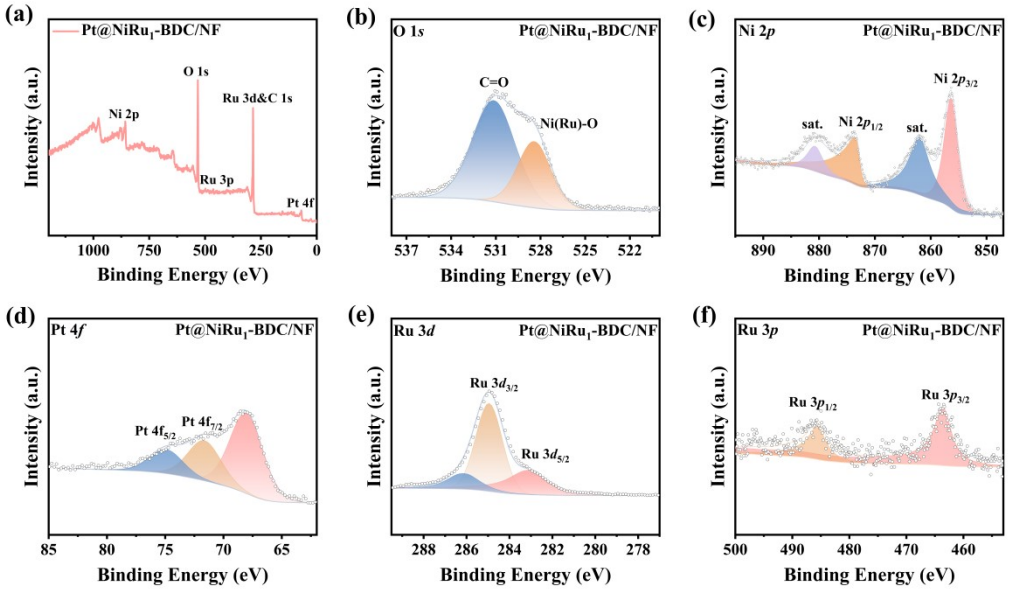


**Figure S18.** High-resolution XPS spectra of (a) XPS survey spectrum; (b) O 1s; (c) Ni 2p; (d) Pt 4f; (e) Ru 3d and (f) Ru 3p for Pt@NiRu$_1$-BDC/NF after MOR cyclic stability test.

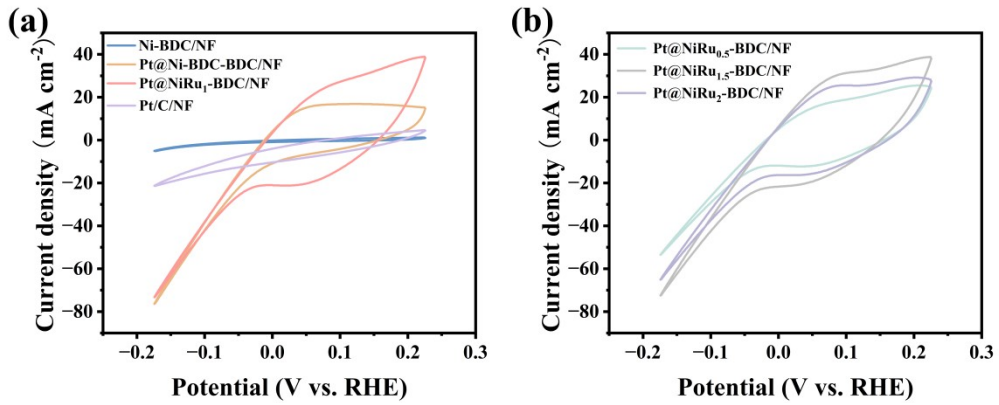


**Figure S19.** CV curves of (a) Ni-BDC/NF, Pt@Ni-BDC/NF, Pt@$NiRu_1$-BDC/NF, and Pt/C electrocatalysts and (b) Pt@$NiRu_{0.5}$-BDC/NF, Pt@$NiRu_{1.5}$-BDC/NF, and Pt@$NiRu_2$-BDC/NF.

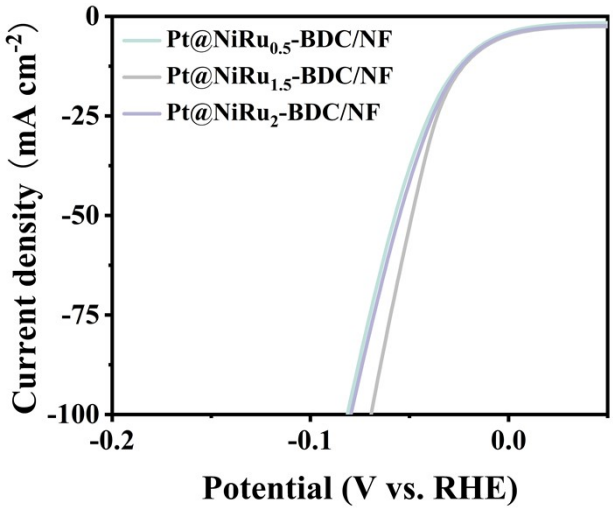


**Figure S20.** LSV curves of Pt@$NiRu_{0.5}$-BDC/NF, Pt@$NiRu_{1.5}$-BDC/NF and Pt@$NiRu_2$-BDC/NF.

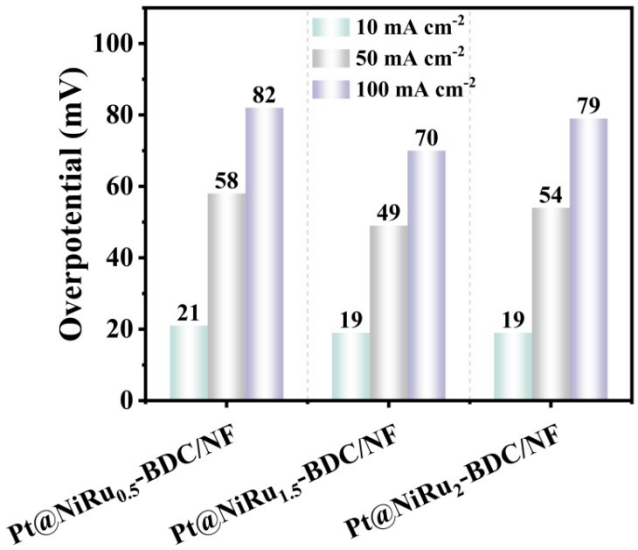


**Figure S21.** Overpontials of Pt@$NiRu_{0.5}$-BDC/NF, Pt@$NiRu_{1.5}$-BDC/NF, and Pt@$NiRu_2$-BDC/NF at the current density of 10, 50, and 100 mA $cm^{-2}$.

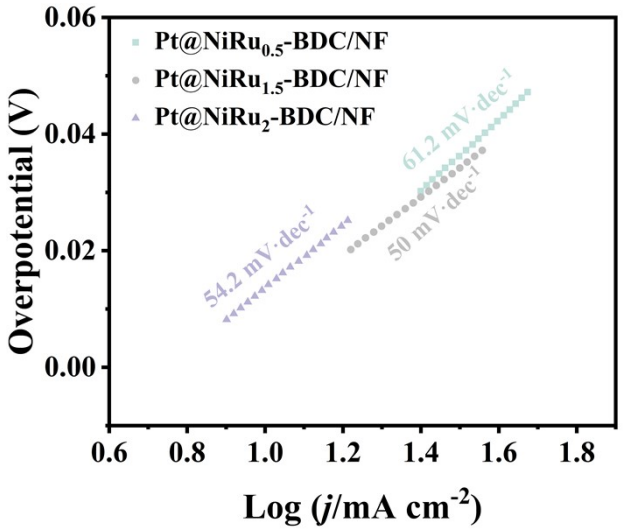


**Figure S22.** Tafel slopes of Pt@$NiRu_{0.5}$-BDC/NF, Pt@$NiRu_{1.5}$-BDC/NF and Pt@$NiRu_2$-BDC/NF.

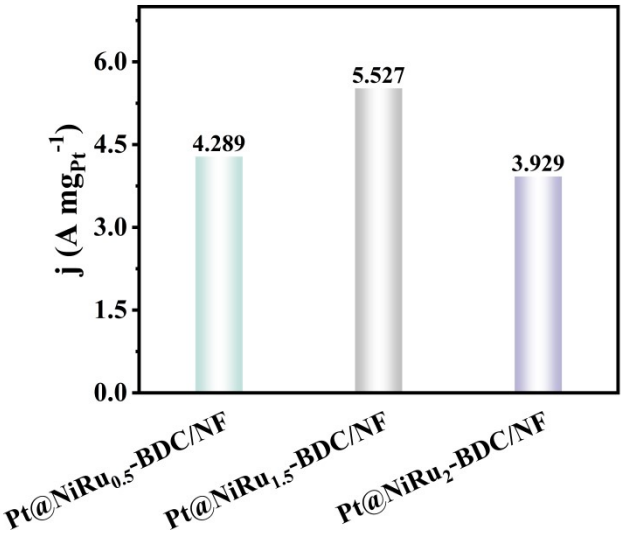


**Figure S23.** HER mass activity for Pt@$NiRu_{0.5}$-BDC/NF, Pt@$NiRu_{1.5}$-BDC/NF and Pt@$NiRu_2$-BDC/NF electrocatalysts.

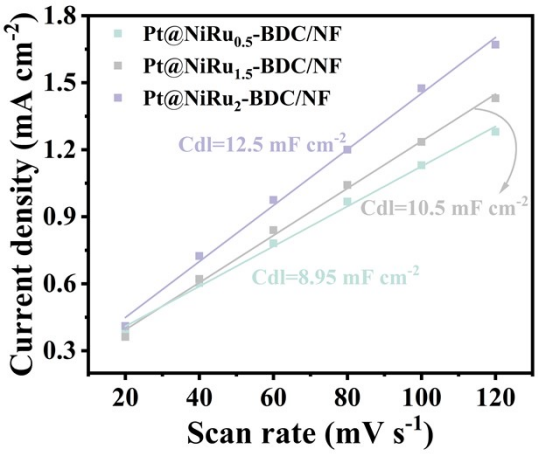


**Figure S24.** Double-layer capacitance of Pt@NiRu$_{0.5}$-BDC/NF, Pt@NiRu$_{1.5}$-BDC/NF, and Pt@NiRu$_2$-BDC/NF.

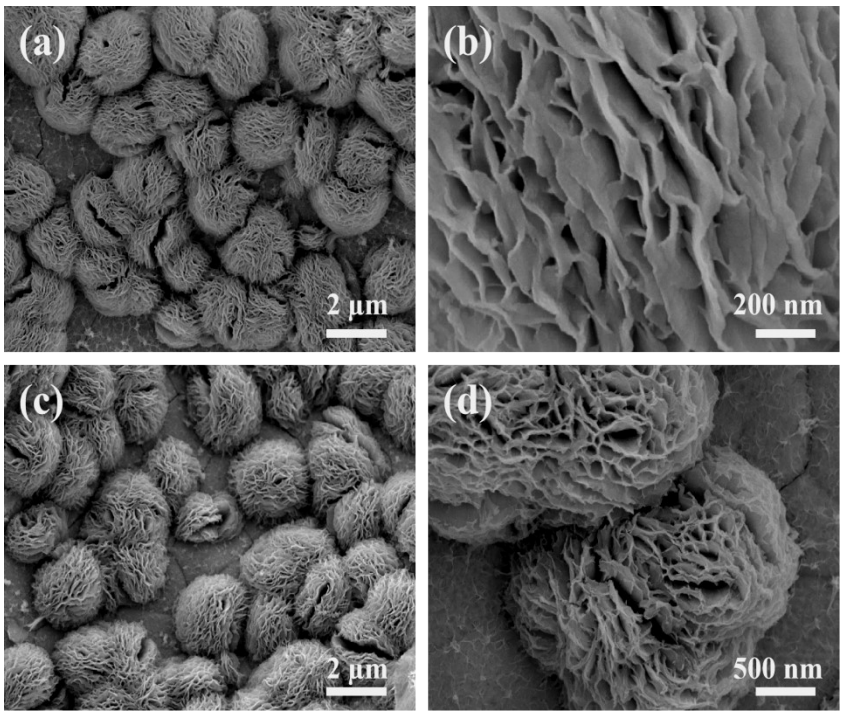


**Figure S25.** SEM images of Pt@NiRu$_1$-BDC/NF after (a, b) 1000 CV cycles and (c, d) 10000 CV cycles.